

# Dynamic interdependence and competition in multilayer networks

Michael M. Danziger<sup>1,5\*</sup>, Ivan Bonamassa<sup>2,5</sup>, Stefano Boccaletti<sup>3,4</sup> and Shlomo Havlin<sup>2</sup>

**From critical infrastructure to physiology and the human brain, complex systems rarely occur in isolation. Instead, the functioning of nodes in one system often promotes or suppresses the functioning of nodes in another. Structural interdependence—that is, when the functionality of the nodes is determined exclusively by connectivity between layers—can be characterized via percolation processes on interdependent networks. However, modelling more general interactions between dynamical systems has remained an open problem. Here, we present a dynamic dependency framework that can capture interdependent and competitive interactions between dynamic systems, which we use to study synchronization and spreading processes in multilayer networks with interacting layers. By developing a mean-field theory, which we verify by simulations, we find coupled collective phenomena, including multistability, regions of coexistence, and macroscopic chaos. In interdependent dynamics, in particular, we observe hysteretic behaviours with abrupt (hybrid and explosive) transitions, that exhibit universal features that match those emerging from interdependent percolation. This dynamic dependency framework provides a powerful tool with which to improve our understanding of many of the interacting complex systems surrounding us.**

Many real-world complex systems include macroscopic subsystems which influence one another. This arises, for example, in competing or mutually reinforcing neural populations in the brain<sup>1–3</sup>, spreading dynamics of viruses<sup>4</sup> or opinions<sup>5</sup>, and elsewhere<sup>6,7</sup>. It is therefore important to understand how different types of inter-system interaction can influence the overall collective behaviour.

In 2010, substantial progress was made when the theory of percolation on interdependent networks was introduced<sup>8,9</sup>. This model showed that when nodes in one network depend on nodes in another to function, catastrophic cascades of failures and abrupt structural transitions arise, as observed in real-world systems<sup>10–12</sup>. However, interdependent percolation is limited to systems where functionality is determined exclusively by connectivity, thus providing only a partial understanding of real-world systems, where the network serves as the base on which dynamic processes occur.

Two fundamental and ubiquitous ways in which nodes in one system can influence nodes in another one are interdependence, as in critical infrastructures<sup>13</sup> or financial networks<sup>14,15</sup>, and competition, as observed in ecological systems<sup>16,17</sup>, social networks<sup>5</sup>, or in the human brain<sup>1,18</sup>. Interdependent and competitive interactions may also occur simultaneously, as observed in predator–prey relationships in ecological systems<sup>19</sup>, and in binocular rivalry in the brain<sup>20</sup>. Recent work by Nicosia et al.<sup>18</sup> showed how the two processes of diffusion and synchronization can intertwine on a multiplex network, and how the phase space is impacted, including the possibility of explosive transitions. Special cases of cooperative<sup>21,22</sup>, antagonistic<sup>23–27</sup> and asymmetric interactions<sup>28–30</sup> between networks have been studied, but without a general framework capable of unveiling universal patterns.

Here we introduce a general framework where we define cross-system dependency links by multiplying the coupling strength of a node to its neighbours in one network by a function of the instantaneous local order of a node in another, which we take as a proxy for its functionality (Fig. 1). If the function is increasing (decreasing),

then the potential for local order of the two nodes is positively (negatively) correlated, reflecting an interdependent (competitive) interaction. Because local order can be meaningfully defined for a wide range of statistical mechanical models, this framework can capture an unprecedented variety of coupled collective phenomena.

We apply our general approach to a system of two networks of Kuramoto oscillators and a system of two reversible (susceptible–infected–susceptible (SIS)) epidemic processes, with different combinations of competitive and interdependent interactions. We find that under an interdependent interaction, the systems exhibit collective behaviours familiar from interdependent percolation: abrupt phase transitions from order to disorder, and universal critical dynamics during collapse. Furthermore, because of the added richness of the dynamical models, we observe new features such as forward (explosive) transitions from disorder to order and hysteresis. Similarly, under a competitive interaction, we find regions of coexistence, hysteresis and multistability. When the two types of interaction are asymmetrically implemented, we observe novel collective phases and macroscopic chaotic behaviours. Because the couplings are expressed via local order functions, we are able to perform a mean-field approximation of the exact equations, which are solved numerically and verified with excellent agreement against extensive simulations on large synthetic networks.

## Model

We begin by considering isolated dynamical systems composed of  $N$  nodes which evolve according to

$$\dot{x}_i = g_i(x_i) + \lambda \sum_{j=1}^N A_{ij} h(x_j, x_i) \quad (1)$$

where  $x_i$  is the dynamic state of node  $i$ ,  $g_i$  and  $h$  are scalar-valued functions of self-dynamics and pairwise interactions, respectively,

<sup>1</sup>Department of Physics, Northeastern University, Boston, MA, USA. <sup>2</sup>Department of Physics, Bar-Ilan University, Ramat Gan, Israel. <sup>3</sup>CNR - Institute for Complex Systems, Sesto Fiorentino, Italy. <sup>4</sup>Unmanned Systems Research Institute, Northwestern Polytechnical University, Xi'an, China. <sup>5</sup>These authors contributed equally to this work: Michael M. Danziger, Ivan Bonamassa \*e-mail: [m.danziger@northeastern.edu](mailto:m.danziger@northeastern.edu)

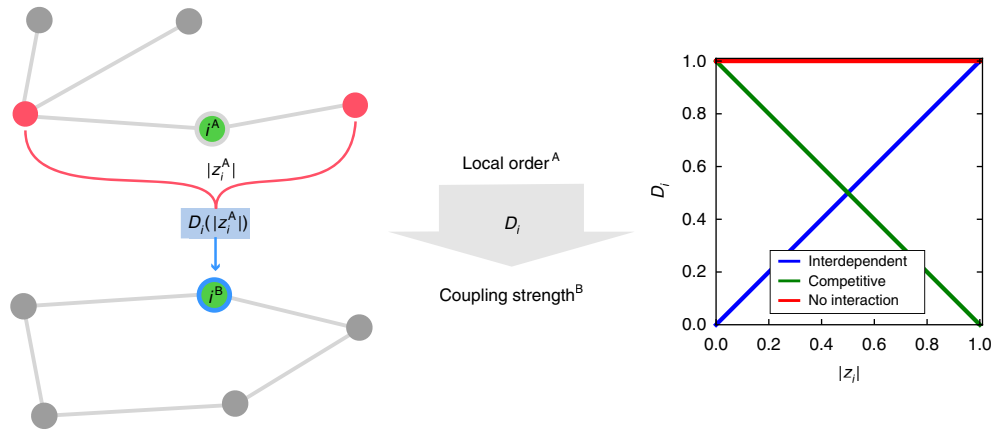


**Fig. 1 | Dynamic interdependence and competition.** (Left) The process-based state of node  $i$  in network A is characterized by the local order  $z_i^A$  measured over its nearest neighbours (see below and Supplementary Section 5 for more general interactions). This quantity modifies the coupling strength of node  $i$  in network B, according to a function  $\mathcal{D}_i^{A \rightarrow B}$  of  $z_i^A$ , which can reflect cooperative, antagonistic or other interactions. Note that there are typically interactions in the opposite direction as well (that is,  $\mathcal{D}_i^{B \rightarrow A}$ ), which have been omitted from this drawing for clarity. (Right) Summary of the dynamical interaction strategies considered here: interdependence (blue), competition (green) and no interactions (red).

$\lambda$  is a coupling strength and the network of interactions is represented by the adjacency matrix entries  $A_{ij}$ , which are equal to one if nodes are connected and zero otherwise<sup>31</sup>. This family of models can exhibit thermodynamic phase transitions between disordered and ordered phases, characterized by the global order parameter  $Z(t) := \sum_{i,j} A_{ij} z_i(t) / \sum_{i,j} A_{ij}$ , where

$$z_i(t) := \frac{1}{k_i} \sum_{j=1}^N A_{ij} \mathcal{O}_j(t) \quad (2)$$

are local observables, measuring the instantaneous order around each dynamical unit, with  $k_i = \sum_j A_{ij}$  as the degree of connectivity of node  $i$ , and with  $\mathcal{O}_i \equiv \mathcal{O}(x_i)$  as a system-dependent ordering function.

We now consider the following question: how can a dependency relationship be defined between dynamical systems such as these? To this aim, we seek a process-based definition of a node’s local state that quantifies its functionality, which can then be used to promote or suppress the onset of functionality in another system. As explained in Supplementary Section 5, the local order is an effective and mathematically convenient proxy for quantifying the local functionality of nodes. We thus propose to model a dependency link between dynamical units via multiplication of the coupling strength  $\lambda$  of a node in one network by a function of the local order parameter  $z_i(t)$  in another:

$$\lambda_B \rightarrow \lambda_B \mathcal{D}_i^{A \rightarrow B}(t) \quad (3)$$

where  $\mathcal{D}_i^{A \rightarrow B}$  is a function of  $z_i^A(t)$ . Because the labelling of the nodes is arbitrary, we assume that node  $i$  in layer A affects node  $i$  in layer B. Alternatively,  $x_i^A$  and  $x_i^B$  can be taken to represent different features of the same node in a multiplex, where different layers reflect different dynamics and hence different node states. As demonstrated in Fig. 1, a suitable choice of  $\mathcal{D}_i$  can represent an interdependent or a competitive interaction. Here we consider

$$\mathcal{D}_i^{A \rightarrow B}(t) = \begin{pmatrix} |z_i^A|(t) & \text{interdependent} \\ 1 - |z_i^A|(t) & \text{competitive} \\ 1 & \text{decoupled} \end{pmatrix} \quad (4)$$

and leave more exotic interactions for future study.

In this manner, we can describe the evolution of the  $i$ th dynamic unit in layer  $\sigma$  of an  $M$ -layered ensemble interacting networked dynamical systems with the equations:

$$\dot{x}_i^\sigma = g_i(x_i^\sigma) + \lambda_\sigma \prod_{\mu=1}^M \mathcal{D}_i^{\mu \rightarrow \sigma} \sum_{j=1}^N A_{ij}^\sigma h(x_i^\sigma, x_j^\sigma) \quad (5)$$

where the  $g_i$  and  $h$  functions are assumed to be the same in each network—that is, the same process is taking place on each layer—and the two processes have equal timescales. We relax these assumptions in Supplementary Section 4, where we address the case of interactions between entirely different processes. Without loss of generality, the node ordering is chosen so that the nodes  $i$  in each layer interact with each other. The product in equation (5) reflects the assumption that if the interaction term  $\mathcal{D}_i^{\mu \rightarrow \sigma}$  goes to zero in any of the layers, it suppresses the coupling of node  $i$  in every layer, reflecting mutual interdependence (or competition). We can thus consider each  $\mathcal{D}_i^{\mu \rightarrow \sigma}$  term as the  $(\mu\sigma)$ -element of a set of supra-adjacency matrices  $\mathcal{D}_i(t)$  describing the interactions between layers at node  $i$ , which for the case of two interacting networks A and B would be represented as:

$$\mathcal{D}_i(t) = \begin{pmatrix} 1 & \mathcal{D}_i^{B \rightarrow A}(t) \\ \mathcal{D}_i^{A \rightarrow B}(t) & 1 \end{pmatrix}$$

where we have assumed that there are no self-interactions.

Because each  $\mathcal{D}_i$  is determined entirely by the local order parameters (equation (2)), it is straightforward to analyse the inter-system dynamics of the model equation (5) within a heterogeneous mean-field theory (see Methods and Supplementary Information for further details), where each  $z_i^\sigma$  is replaced by the corresponding global quantity  $Z_\sigma$ . For many physical systems described by equation (1), this approach enables the solution of the collective properties of equation (5) in terms of a low-dimensional system of equations. For two networks, we can derive a general system of coupled self-consistent equations for  $(Z_A, Z_B)$  in the stationary regime, which in the continuous limit reads

$$Z_\sigma = \int_{k_{\min}}^{+\infty} \frac{k P_\sigma(k)}{\langle k \rangle_\sigma} \mathcal{G}_\sigma(\lambda_\sigma | Z_\sigma | \mathcal{D}^{\mu \rightarrow \sigma}, k) dk \quad (6)$$

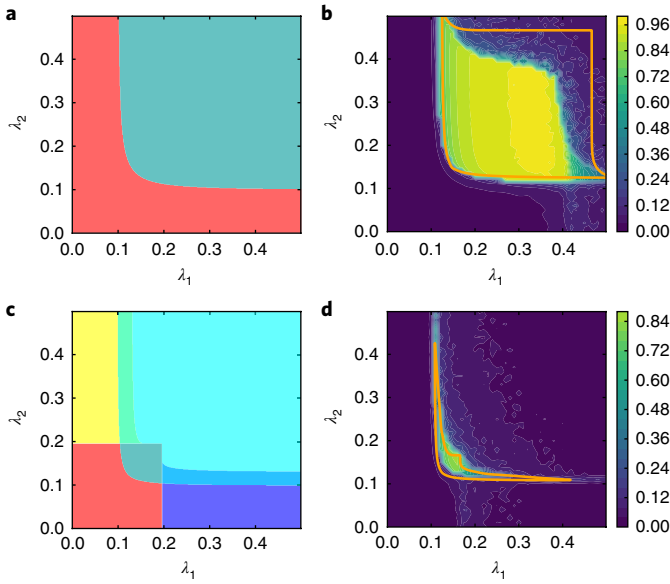


**Fig. 2 | Interdependent synchronization.** **a**, Mean-field phase diagram for fully ( $f=1$ ) interdependent ER ( $\langle k \rangle = 12$ ) networks of Kuramoto oscillators. There are two regions: red where no network is synchronized, and cyan-on-red where both synchronized and desynchronized solutions are stable. **b**, Difference in final synchronization depending on initial conditions for systems of size  $N = 2^{13}$ . The yellow area represents the metastable region found in simulations and the orange line its mean-field prediction, having accounted for fluctuations of the coherences of nominal size  $\Delta R \approx 0.2$ . **c**, Predicted phase diagram for partially ( $f=1/2$ ) interdependent ER networks. In addition to the phases shown in **a**, we have network 1 (2) only marked in blue (yellow), which coexists with the both-synchronized solution where the cyan region overlaps. Additionally, we have a cyan-only region where the zero-solution is now unstable. **d**, The metastable region and its mean-field prediction for the partially interdependent case.

where  $\mathcal{D}^{\mu \rightarrow \sigma}$  equals the mean-field term ( $|Z_\mu|$  for interdependent and  $1 - |Z_\mu|$  for competitive interactions),  $\mathcal{G}_\sigma$  is a dynamics-dependent function based on the mean-field solution of the single layer case, and  $P_\sigma$  is the degree distribution of the layer  $\sigma = A, B$ . The networks are not required to have the same topology, but we assume both of them to belong to the uncorrelated configuration model. Note also that equation (6) holds when all the dynamical units in each layer are mutually (one-to-one) coupled. In Methods, we provide the generalized equation for the case where only fractions  $f_A, f_B < 1$  of randomly chosen nodes are dynamically coupled.

We now apply our framework to Kuramoto oscillators and reversible (SIS) epidemics in three configurations: mutually interdependent; mutually competitive; and one way interdependent and one way competitive (asymmetric). All three cases have real-world motivations, and are studied with full ( $f=1$ ) and partial ( $f < 1$ ) couplings.

**Interdependent and competitive synchronization.** Synchronization is a common phenomenon observed in diverse systems<sup>32</sup>. Its spontaneous onset in populations of phase oscillators, in particular, has been the subject of intense research after the seminal papers by Winfree<sup>33</sup>, and especially by Kuramoto, whose model we investigate hereafter<sup>34,35</sup>.

In the Kuramoto model, oscillators' phases  $\theta_i \in [0, 2\pi)$  evolve according to a system of equations of the form given in equation (1), where  $g_i(\theta_i) = \omega_i$  maps each node to its natural frequency and  $h(\theta_j, \theta_i) = \sin(\theta_j - \theta_i)$ . Following equation (5), we model the cross-system dynamics of two dependent networks of Kuramoto oscillators as

$$\dot{\theta}_i^\sigma = \omega_i^\sigma + \lambda_\sigma \mathcal{D}_i^{\mu \rightarrow \sigma} k_i^\sigma \text{Im}(z_i^\sigma e^{-i\theta_i^\sigma}) \quad (7)$$

where the functions  $\mathcal{D}_i$  are defined according to equation (4), and the local order parameters  $z_i \equiv r_i e^{i\theta_i}$  as in equation (2) with  $\mathcal{O}_i = e^{i\theta_i}$ . In the form of equation (7), the oscillators interact only through  $z_i$  and  $\mathcal{D}_i$ , which produces feedback between the synchronization states (see Supplementary Section 5.1.2) of nodes in different layers. Being otherwise decoupled, equation (7) can be solved using the heterogeneous mean-field theory, yielding the self-consistent equation (6) for the global coherences  $R_\sigma = |Z_\sigma|$  with  $\mathcal{G}_\sigma^{\text{Kura}}(y, k) \equiv \int_{-ky}^{ky} u_\sigma(\omega) \sqrt{1 - \omega/k y} d\omega$ , where the  $u_\sigma$  are the distribution of the oscillators' natural frequencies, assumed to be unimodal and symmetric around zero. In Methods and Supplementary Sections 2 and 5.1.2 we extend the results to arbitrary frequency distributions and partial couplings. For simplicity, we analyse the symmetric case, with  $u_A \equiv u_B$  uniform and Erdős–Rényi (ER) nets with equal average degree.

We first consider the interdependent case, where the dynamics follows equation (7), where  $\mathcal{D}_i^{\mu \rightarrow \sigma} = r_i^\mu$  for a fraction  $f$  of the nodes. Since the local synchronizabilities of both networks are positively correlated, we observe collective patterns resembling the mutual giant component in interdependent percolation<sup>8</sup>. In particular, for any  $f \neq 0$ , we find that the global synchronization levels undergo discontinuous desynchronization transitions as the coupling strengths are decreased. However, unlike percolation models, we can now investigate the forward (that is, disorder-to-order) transition, where a giant synchronized cluster might spontaneously emerge. When  $f=1$ , we find that the incoherent phase is absorbing, and becomes unstable only because of the existence of a nearby saddle point (Fig. 2a and Supplementary Fig. 2) and large enough fluctuations due to the quenched disorder of the natural frequencies (Fig. 2b and Supplementary Fig. 1). For  $f < 1$ , the desynchronized phase becomes unstable even in the thermodynamic limit, and the system spontaneously jumps to the synchronized branch (Fig. 2c and Supplementary Fig. 4) after crossing the metastable region (Fig. 2d and Supplementary Fig. 3).

These abrupt forward transitions and hysteretic patterns are absent in the classical Kuramoto model, and have been reported earlier in the context of explosive synchronization<sup>36,37</sup>, or in modelling amplification mechanisms in cavity-coupled Josephson junctions<sup>38</sup>.

Turning to the case of competitive synchronization, which is relevant for competing neural populations<sup>1</sup>, in particular in multistable perception<sup>39</sup> or visual processing of optical illusions<sup>40</sup>, we can follow the same steps as above but with  $\mathcal{D}_i = 1 - r_i$ . This system shows pronounced metastability without phase coexistence for  $f=1$  (Supplementary Figs. 5 and 6) and intriguing coupled collective phenomena when  $f < 1$ . In addition to the simple states of global incoherence or domination by one network on the other, we find chimera-like regimes (purple and green regions in Fig. 3a) in which the decoupled nodes synchronize whereas the competitively coupled nodes remain desynchronized, leading to a partial synchronization level bounded by  $f$ , with a two-stage transition between the phases (Fig. 3b). Following alternative paths in the mean-field phase diagram, we observe other non-trivial transitions (Supplementary Fig. 9). We further find quadrastability for a small region of the phase space (Fig. 3a and Supplementary Figs. 7 and 8), whose existence depends on the frequency distribution adopted (see Supplementary Section 2.2 and Supplementary Fig. 10d).

Finally, we consider the asymmetric case, in which the synchronization of nodes in network A suppresses the onset of synchronization of nodes in network B, while synchronization in network B enhances the synchronizability in network A (see Supplementary Section 2.2). Similar behaviour is observed in binocular rivalry, in which neurons associated with the dominant eye synchronize more strongly when the weak eye is stimulated, but the weak eye synchronizes less strongly when the dominant eye is stimulated<sup>20</sup>. We find spiral sink solutions when  $f < 1$  (Fig. 4a–c), and macroscopic chaos when  $f=1$  (Fig. 4d, e). The chaotic behaviour is due to oscillations

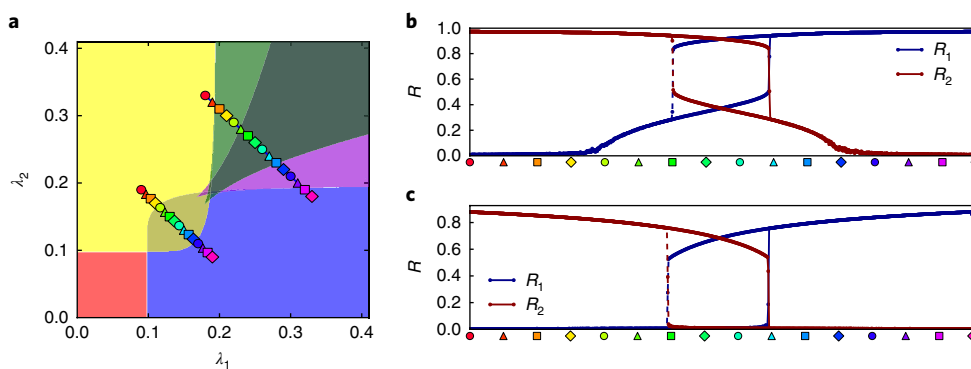


**Fig. 3 | Competitive synchronization.** **a**, Mean-field phase diagram for two partially ( $f=0.5$ ) competitive ER networks ( $\langle k \rangle = 12$ ) of Kuramoto oscillators. **b**, Two-stage transition (upper line in **a**). The system transitions continuously between the state where only one network synchronizes to the state where one dominates but the other has partial synchronization (yellow-green and blue-purple), and then discontinuously as the fully synchronized network drops to partial synchronization and the partially synchronized one becomes fully synchronized (green-purple and purple-green in the overlapping region). **c**, Single-stage transition (lower line in **a**). When leaving the metastable region (yellow-blue overlapping region), the synchronization of one network drops to zero while the other jumps to a large finite value. Results obtained by numerically integrating equation (7) with  $\mathcal{D}_i = 1 - r_i$ , for networks of size  $N = 2^{17}$ .

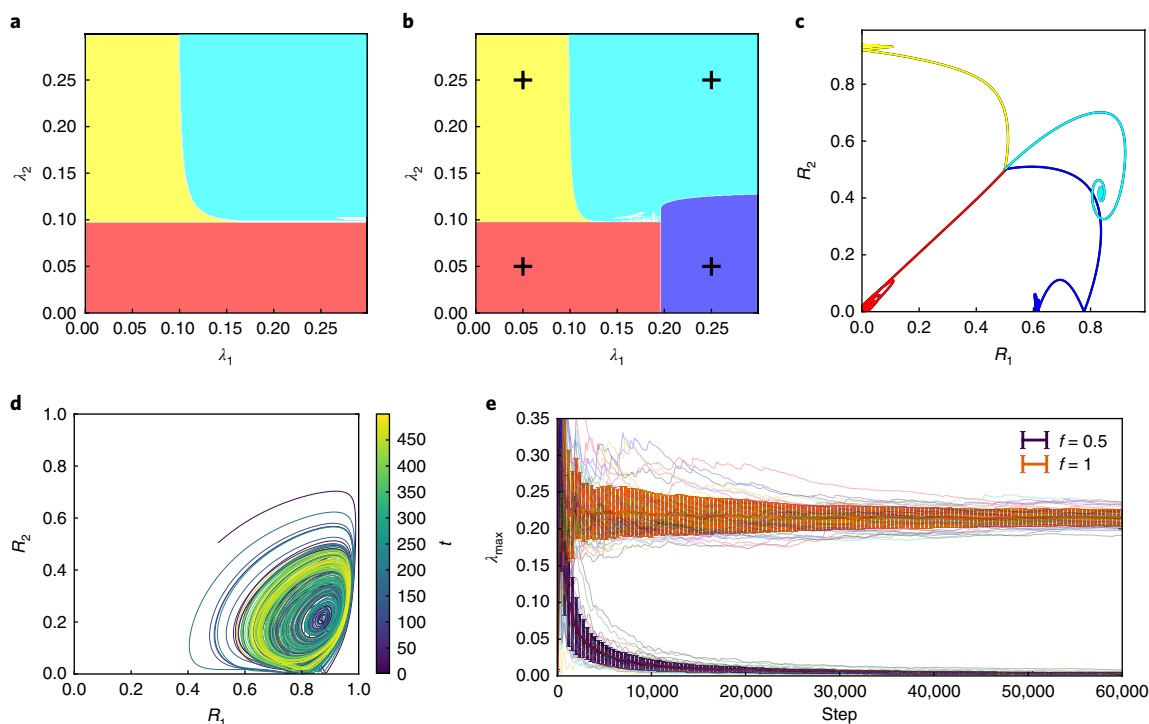


**Fig. 4 | Asymmetric synchronization.** **a**, Phase diagram for the fully ( $f=1$ ) interacting case. **b**, Partially ( $f=1/2$ ) interacting case. **c**, State-space trajectories for systems corresponding to the locations marked in **b**. Note the spiral sink (cyan) solution, where both networks are synchronized. For each point, the system is initialized at the same synchronization level and integrated for  $t=500$  for ER networks with  $\bar{k} = 12$  and  $N = 2^{21}$ . **d**, Sample of a typical trajectory showing macroscopic chaos in full ( $f=1$ ) asymmetric synchronization. **e**, Estimate of the largest Lyapunov exponent  $\lambda_{\max}$  for the chaotic trajectories in **d** for systems of size  $N = 2^{15}$ , calculated as described in ref. <sup>58</sup>. Averaging over 50 runs, we find  $\lambda_{\max} = 0.21 \pm 0.01$  for  $f=1$ , in contrast with the converging behaviour for  $f=1/2$ , where  $\lambda_{\max} < 10^{-3}$ .

in the order parameter causing oscillations in the effective coupling term, which is known to lead to chaos<sup>41</sup>.

Besides the rich and realistic patterns uncovered, a unique advantage of our model is that, because the coupling between the networks is on the level of order and not of phase, we are now able to model the cooperative onset of synchronization at different frequency bands. This is significant in light of the complex interactions

between neural populations of different frequencies<sup>42,43</sup>, which cannot be captured by existing multilayer models<sup>44,45</sup>, and the potential for understanding learning tasks<sup>46</sup>, modelling fundamentally multi-frequency phenomena such as hearing<sup>47</sup> and physiological synchronization among organ systems in the body<sup>48</sup>.

With the future aim of addressing these phenomena using the idea of order affecting order, we have applied our framework to networks

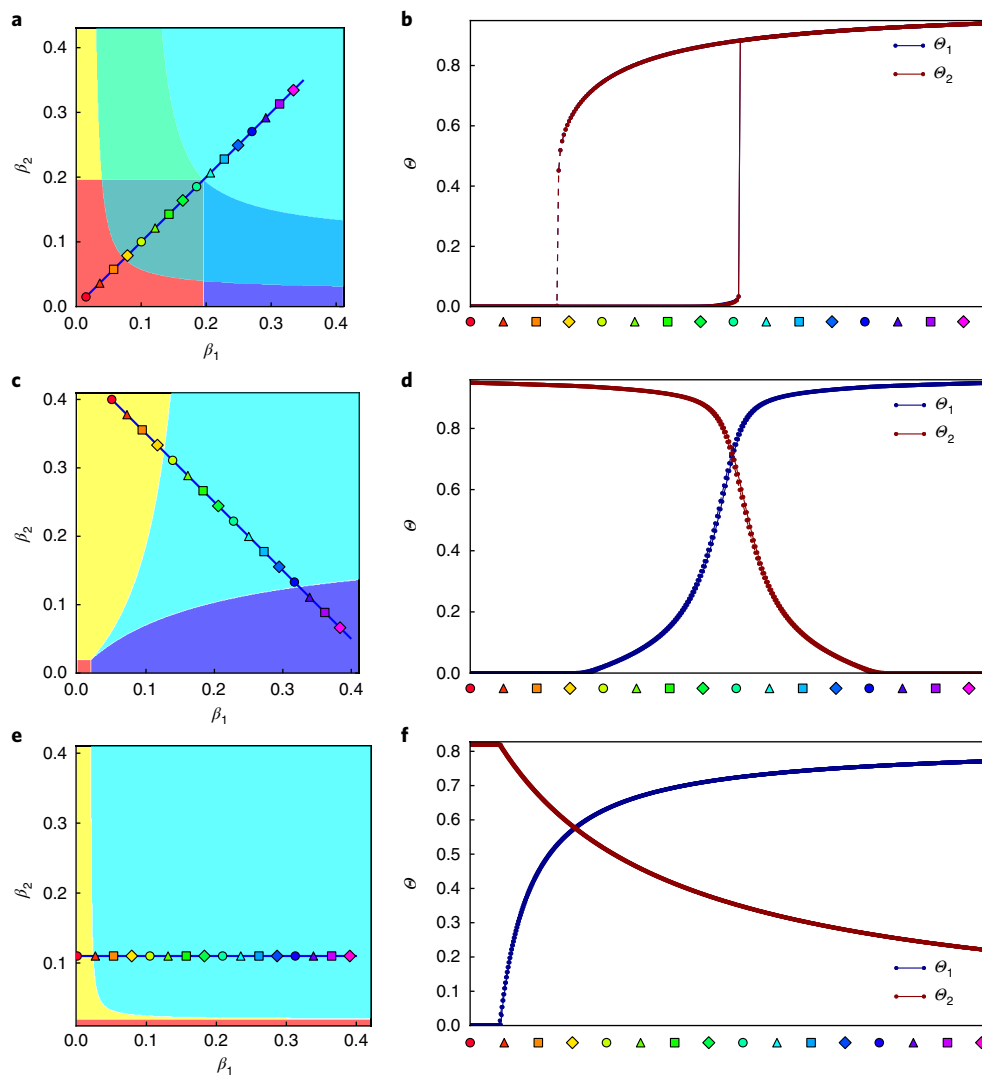


**Fig. 5 | Interacting epidemics.** Interacting SIS dynamics on ER networks with  $\langle k \rangle = 50$ , for partial ( $f = 0.9$ ) interdependent and competitive interactions. **a**, Interdependent phase diagram. The mean-field solution of equation (8) based on equation (12) yields four phases: yellow (only network 2 infected), blue (only network 1 infected), cyan (both networks infected) and red (healthy phase). Overlapping areas unveil three regions of bistability. **b**, Hysteresis. Integrating the full system along the main diagonal depicted in **a**, we obtain the predicted hysteric pattern. Blue and red curves are almost indistinguishable because the system is symmetric with respect to the networks' settings. **c**, Competitive phase diagram. Phases follow the same colour legend as in **a**. Note the absence of multistable regimes. **d**, Coexistence. As in **b**, but following the anti-diagonal phase path depicted in **c**. We observe the spontaneous emergence of a coexistence regime (which extends itself through all the cyan area in **c**), where neither epidemic dominates, but both them infect significant fractions of the networks. Here the forward and backward curves perfectly overlap, because there is no metastability. **e**, Mean-field phase diagram for asymmetric SIS dynamics. **f**, In the asymmetric case, the disease level can be decreased substantially just by increasing the communicability in the other layer. System size for numerical results is  $N = 10^3$ .

of Winfree oscillators (see Methods and Supplementary Section 2). In this way, going beyond the weak-coupling limit of Kuramoto-like models, we can naturally incorporate pulse-like interactions and phase-response curves, commonly obtained from experiments.

**Interacting epidemics.** Epidemic models are another important family of dynamical processes where the model in equation (5) can be successfully applied. Multiple diseases or strains can spread cooperatively<sup>21,22,49</sup>, with the onset of one disease increasing the susceptibility to contract others, or antagonistically<sup>23,50</sup>, as in cross-immunization processes, where the contraction of an infection increases the resilience of its host in contracting another. At the same time, if awareness (and an immunizing response) of the infection spreads among the same agents via their social network, the disease layer can enhance the immunizing awareness layer even

as the latter suppress the former<sup>28,29,51</sup>. Several attempts have been made so far to cast these diverse settings and ad-hoc models into a unified framework for interacting epidemics<sup>50,52</sup>. Our work complements these efforts and provides a simpler and more general framework for analysing interacting epidemics in the broader context of dynamical systems.

Here, we consider the SIS model<sup>53</sup>, whose dynamics in an isolated network is represented by  $\dot{x}_i = -\gamma x_i + \beta(1-x_i) \sum_j A_{ij} x_j$ , where  $\gamma, \beta \in [0,1]$  are the recovery and infection rates of the process, respectively, and  $x_i$  is the probability that node  $i$  is infected. With  $\mathcal{O}(x) \equiv x$  for the ordering function, a set of local fields  $\Theta_i$  can be defined according to equation (2), leading to the epidemics analogue of equation (5):

$$\dot{x}_i^\sigma = -x_i^\sigma + \beta_\sigma \mathcal{D}_i^{\mu \rightarrow \sigma} k_i^\sigma \Theta_i^\sigma (1-x_i^\sigma) \quad (8)$$

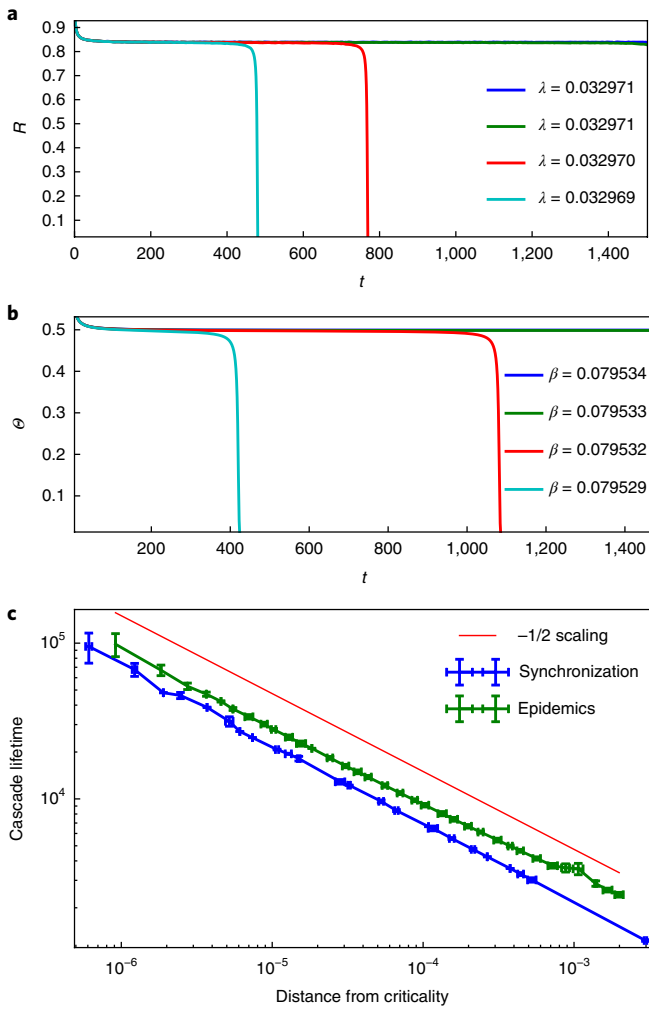


**Fig. 6 | Universal scaling in interdependent dynamics. a, b,** Below the critical thresholds at which the abrupt backward (order-to-disorder) transitions take place, the collective behaviours of interdependent systems are characterized by slow transient dynamics with universal features. Here the system’s state spends the bulk of its relaxation time, with the order parameter maintaining an approximately constant value (the ‘plateau’ stage), before collapsing exponentially to the disordered phase. This process is comparable in (either partially or fully) interdependent synchronization of Kuramoto oscillators (**a**) and epidemics in SIS processes (**b**). **c,** From the theory of dynamical systems<sup>59</sup>, we expect that the time spent by the trajectory of the state to pass the bottleneck created by the remnant of a saddle-node bifurcation scales with an exponent of  $-1/2$  below criticality, which we observe in both systems above the backward transitions. The x axis is  $\lambda_c - \lambda$  ( $\beta_c - \beta$ ) for the synchronization (epidemic) data. The same exponent is observed near the hybrid transitions reported in interdependent percolation<sup>8</sup> and in  $k$ -core pruning processes<sup>55</sup>. Results are obtained for ER networks with  $\langle k \rangle = 50$ ,  $N = 2 \times 10^3$  for SIS epidemics and  $N = 2^{15}$  for Kuramoto oscillators, averaged over 20 runs. Error bars show standard deviations around means, calculated from all points in each logarithmically spaced interval.

for two SIS processes, where the couplings  $\mathcal{D}_i$  activate local feedback between the nodes’ epidemic state (see Supplementary Section 5.1.1), and hence of the networks’ infectious levels. Note that in writing equation (8) we assumed for simplicity  $\gamma_\sigma \equiv 1$  so that the two processes have equal timescales.

Applying the heterogeneous mean-field theory shown in Methods to equation (8), we obtain a self-consistent solution for  $(\Theta_A, \Theta_B)$  in equation (6), where now  $\mathcal{G}_\sigma^{\text{SIS}}(y, k) = ky/(1 + ky)$ . Looking at the results of these interactions on ER networks, we recover many relevant phenomena recently reported in the literature, and also find novel ones. In the interdependent case, we find hybrid phase transitions for  $f=1$  (Fig. 5a) and hysteretic behaviour with abrupt forward and backward transitions (Fig. 5c,d) whenever  $f < 1$ . In practical terms, the existence of abrupt forward transitions exposes the system to the risk of explosive pandemics<sup>22,52</sup>, which might happen without warning. On the other hand, interventions which lower  $\beta$  during endemic infections can trigger cascades of eradication which can abruptly jump the system to its healthy phase. However, the hysteretic property means that it is much harder (that is, requires reducing communicability to a lower value) to eradicate an outbreak than it is to keep it from breaking out. Finally, a consequence of the bistability observed when  $f=1$  (red-on-cyan phase in Fig. 5a) is that, in sharp contrast to isolated SIS epidemics, the healthy state has a finite basin of stability (Fig. 5b and Supplementary Fig. 13), meaning that small outbreaks are expected to die out even for comparatively high transmission rates.

In the competitive case we find behaviours which differ from the ones observed in synchronization. Instead of metastability and abrupt transitions, we find that partially competing diseases continuously transition from mutual exclusion behaviours to broad coexistence regimes (Fig. 5e, f and Supplementary Fig. 14) where neither disease excludes the other and both reach epidemic proportions<sup>50</sup>, presenting a challenge to optimize cross-immunization strategies. For asymmetric couplings, the mean-field predictions (Supplementary Fig. 11c, d) resemble the ones uncovered in the synchronization case (Fig. 4a, b). We observe a broad region of coexistence and phase-paths-dependent cooperative behaviours, a direction so far overlooked in the epidemic community, that reflect intriguing three-stage awakening transitions (see Supplementary Fig. 15) where the immunizing layer is first ‘awakened’ by the outbreak from the diseased state, and eventually transitions spontaneously to the healthy phase. In particular, when  $f=1$  we observe that more than the 75% of the network can be healed just by increasing the transmission of awareness (Fig. 5e, f). In contrast with the synchronization case, the system does not display any macroscopic chaotic behaviour but exhibits spiral sink endemic solutions (Supplementary Fig. 16d, h), a novel feature of interacting SIS spreading processes.

**Discussion**

We argue here (and more extensively in Supplementary Section 5) that our model represents a natural generalization of the concept of dependency from percolation to dynamical processes. Equation (3) can be interpreted as a dynamic dependency link since it has the same impact on dynamic-based order that the percolation dependency link has on the connectivity-based order. In particular, when implementing interdependent interactions as in equation (4), we find that as long as node  $i$  is locally disordered in network B (that is,  $|z_i^B| \approx 0$ ), then so is its ‘replica’ in network A, being effectively cut off from its own neighbours. This reflects a dynamical counterpart of interdependent percolation<sup>8</sup>, where the local order of a node is defined as whether any of its neighbours leads to the mutual giant connected component. Like interdependent percolation, dynamic interdependence increases the vulnerability of the system<sup>13</sup>, as reflected in higher critical thresholds and abrupt transitions. In the backward direction, we find that all the above systems exhibit universal dynamics near criticality, characterized by slow transient processes immediately after the transition (Fig. 6). Although these ‘plateau’ stages have been interpreted as critical branching processes in interdependent percolation<sup>54,55</sup>, here we observe them emerging whenever the system is close to a saddle-node bifurcation, whose fingerprint clearly appears

with the square-root scaling  $\tau \sim (\lambda_c - \lambda)^{-1/2}$  (Fig. 6c). When  $f=1$ , the saddle-node is the only bifurcation, resulting in a hybrid phase transition, as in interdependent percolation<sup>56</sup>. For  $f < 1$ , the saddle-node describes the large-amplitude branch of a subcritical bifurcation<sup>57</sup> yielding hysteresis. Therefore, moving in the forward direction, we have been able to explore the effects that dependencies have on the collective dynamics of the system—an elusive task for percolation models with antagonistic or asymmetric interactions—showing the universal emergence of explosive phase transitions.

This generalization of dependent interactions from percolation to dynamical systems allows for the development of new models for neural, social and technological systems that better capture the subtle ways in which different systems can affect one another. Although we focused only on the fundamental interactions of interdependence and competition, more exotic couplings can be described by this framework by suitably replacing the simple linear functions of  $|z_i|$  in equation (4), and more than two layers can be considered. We find that the phenomenology recovers key features of interdependent percolation as well as uncovers new phenomena, not previously linked to inter-system interactions.

### Online content

Any methods, additional references, Nature Research reporting summaries, source data, statements of data availability and associated accession codes are available at <https://doi.org/10.1038/s41567-018-0343-1>.

Received: 14 August 2017; Accepted: 11 October 2018;

Published online: 26 November 2018

### References

1. Fox, M. D. et al. The human brain is intrinsically organized into dynamic, anticorrelated functional networks. *Proc. Natl Acad. Sci. USA* **102**, 9673–9678 (2005).
2. Stumpf, K. et al. Effects of Parkinson's disease on brain-wave phase synchronisation and cross-modulation. *Europhys. Lett.* **89**, 48001 (2010).
3. Mišić, B. et al. Cooperative and competitive spreading dynamics on the human connectome. *Neuron* **86**, 1518–1529 (2015).
4. Vespignani, A. Modelling dynamical processes in complex socio-technical systems. *Nat. Phys.* **8**, 32–39 (2012).
5. Halu, A., Zhao, K., Baronchelli, A. & Bianconi, G. Connect and win: The role of social networks in political elections. *Europhys. Lett.* **102**, 16002 (2013).
6. Angeli, D., Ferrell, J. E. & Sontag, E. D. Detection of multistability, bifurcations, and hysteresis in a large class of biological positive-feedback systems. *Proc. Natl Acad. Sci. USA* **101**, 1822–1827 (2004).
7. Helbing, D. Globally networked risks and how to respond. *Nature* **497**, 51–59 (2013).
8. Buldyrev, S. V., Parshani, R., Paul, G., Stanley, H. E. & Havlin, S. Catastrophic cascade of failures in interdependent networks. *Nature* **464**, 1025–1028 (2010).
9. Gao, J., Buldyrev, S. V., Stanley, H. E. & Havlin, S. Networks formed from interdependent networks. *Nat. Phys.* **8**, 40–48 (2012).
10. Kivela, M. et al. Multilayer networks. *J. Complex Netw.* **2**, 203–271 (2014).
11. Radicchi, F. Percolation in real interdependent networks. *Nat. Phys.* **11**, 597–602 (2015).
12. Klosik, D. F., Grimbs, A., Bornholdt, S. & Htt, M.-T. The interdependent network of gene regulation and metabolism is robust where it needs to be. *Nat. Commun.* **8**, 534 (2017).
13. Danziger, M. M., Shekhtman, L. M., Bashan, A., Berezin, Y. & Havlin, S. in *Interconnected Networks* (ed. Garas, A.) 79–99 (Springer, Cham, 2016).
14. Kenett, D. Y. & Havlin, S. Network science: a useful tool in economics and finance. *Mind Soc.* **14**, 155–167 (2015).
15. Brummitt, C. D. & Kobayashi, T. Cascades in multiplex financial networks with debts of different seniority. *Phys. Rev. E* **91**, 062813 (2015).
16. Hibbing, M. E., Fuqua, C., Parsek, M. R. & Peterson, S. B. Bacterial competition: surviving and thriving in the microbial jungle. *Nat. Rev. Microbiol.* **8**, 15–25 (2009).
17. Coyte, K. Z., Schluter, J. & Foster, K. R. The ecology of the microbiome: Networks, competition, and stability. *Science* **350**, 663–666 (2015).
18. Nicosia, V., Skardal, P. S., Arenas, A. & Latora, V. Collective phenomena emerging from the interactions between dynamical processes in multiplex networks. *Phys. Rev. Lett.* **118**, 138302 (2017).
19. Blasius, B., Huppert, A. & Stone, L. Complex dynamics and phase synchronization in spatially extended ecological systems. *Nature* **399**, 354–359 (1999).
20. Fries, P., Roelfsema, P. R., Engel, A. K., König, P. & Singer, W. Synchronization of oscillatory responses in visual cortex correlates with perception in interocular rivalry. *Proc. Natl Acad. Sci. USA* **94**, 12699–12704 (1997).
21. Newman, M. E. & Ferrario, C. R. Interacting epidemics and coinfection on contact networks. *PLoS One* **8**, e71321 (2013).
22. Chen, L., Ghanbarnejad, F. & Brockmann, D. Fundamental properties of cooperative contagion processes. *New J. Phys.* **19**, 103041 (2017).
23. Newman, M. E. Threshold effects for two pathogens spreading on a network. *Phys. Rev. Lett.* **95**, 108701 (2005).
24. Zhao, K. & Bianconi, G. Percolation on interacting, antagonistic networks. *J. Stat. Mech.* **2013**, P05005 (2013).
25. Gómez-Gardeñes, J., de Domenico, M., Gutiérrez, G., Arenas, A. & Gómez, S. Layer–layer competition in multiplex complex networks. *Phil. Trans. R. Soc. A* **373**, 20150117 (2015).
26. Valdez, L. D., Muro, M. A. D. & Braunstein, L. A. Failure-recovery model with competition between failures in complex networks: a dynamical approach. *J. Stat. Mech.* **2016**, 093402 (2016).
27. Watanabe, S. & Kabashima, Y. Resilience of antagonistic networks with regard to the effects of initial failures and degree–degree correlations. *Phys. Rev. E* **94**, 032308 (2016).
28. Funk, S., Gilad, E., Watkins, C. & Jansen, V. A. The spread of awareness and its impact on epidemic outbreaks. *Proc. Natl Acad. Sci. USA* **106**, 6872–6877 (2009).
29. Granell, C., Gómez, S. & Arenas, A. Dynamical interplay between awareness and epidemic spreading in multiplex networks. *Phys. Rev. Lett.* **111**, 128701 (2013).
30. Kotnis, B. & Kuri, J. Percolation on networks with antagonistic and dependent interactions. *Phys. Rev. E* **91**, 032805 (2015).
31. Barrat, A., Barthélémy, M. & Vespignani, A. *Dynamical Processes on Complex Networks* (Cambridge Univ. Press, Cambridge, 2008).
32. Arenas, A., Daz-Guilera, A., Kurths, J., Moreno, Y. & Zhou, C. Synchronization in complex networks. *Phys. Rep.* **469**, 93–153 (2008).
33. Winfree, A. T. Biological rhythms and the behavior of populations of coupled oscillators. *J. Theor. Biol.* **16**, 15–42 (1967).
34. Kuramoto, Y. in *International Symposium on Mathematical Problems in Theoretical Physics* (ed. Araki, H.) 420–422 (Springer, Berlin/Heidelberg, 1975).
35. Acebrón, J. A., Bonilla, L. L., Vicente, C. J. P., Ritort, F. & Spigler, R. The Kuramoto model: a simple paradigm for synchronization phenomena. *Rev. Mod. Phys.* **77**, 137 (2005).
36. Zhang, X., Boccaletti, S., Guan, S. & Liu, Z. Explosive synchronization in adaptive and multilayer networks. *Phys. Rev. Lett.* **114**, 038701 (2015).
37. Danziger, M. M. et al. Explosive synchronization coexists with classical synchronization in the Kuramoto model. *Chaos* **26**, 065307 (2016).
38. Filatrella, G., Pedersen, N. F. & Wiesenfeld, K. Generalized coupling in the Kuramoto model. *Phys. Rev. E* **75**, 017201 (2007).
39. Sterzer, P., Kleinschmidt, A. & Rees, G. The neural bases of multistable perception. *Trends Cogn. Sci.* **13**, 310–318 (2009).
40. Eagleman, D. M. Timeline: Visual illusions and neurobiology. *Nat. Rev. Neurosci.* **2**, 920–926 (2001).
41. So, P. & Barreto, E. Generating macroscopic chaos in a network of globally coupled phase oscillators. *Chaos* **21**, 033127 (2011).
42. Gans, F., Schumann, A. Y., Kantelhardt, J. W., Penzel, T. & Fietze, I. Cross-modulated amplitudes and frequencies characterize interacting components in complex systems. *Phys. Rev. Lett.* **102**, 098701 (2009).
43. Lowet, E. et al. Input-dependent frequency modulation of cortical gamma oscillations shapes spatial synchronization and enables phase coding. *PLoS Comput. Biol.* **11**, 1–44 (2015).
44. Barreto, E., Hunt, B., Ott, E. & So, P. Synchronization in networks of networks: The onset of coherent collective behavior in systems of interacting populations of heterogeneous oscillators. *Phys. Rev. E* **11**, e1004072 (2008).
45. Um, J., Minnhagen, P. & Kim, B. J. Synchronization in interdependent networks. *Chaos* **21**, 025106 (2011).
46. Reichert, D. P. & Serre, T. Neuronal synchrony in complex-valued deep networks. Preprint at <https://arxiv.org/abs/1312.6115> (2013).
47. Wang, C.-Q., Pumir, A., Garnier, N. B. & Liu, Z.-H. Explosive synchronization enhances selectivity: example of the cochlea. *Front. Phys.* **12**, 128901 (2016).
48. Bashan, A., Bartsch, R. P., Kantelhardt, J. W., Havlin, S. & Ivanov, P. C. Network physiology reveals relations between network topology and physiological function. *Nat. Commun.* **3**, 702 (2012).
49. Pawlowski, A., Jansson, M., Sköld, M., Rottenberg, M. E. & Källénus, G. Tuberculosis and HIV co-infection. *PLoS Pathog.* **8**, e1002464 (2012).
50. Sanz, J., Xia, C.-Y., Meloni, S. & Moreno, Y. Dynamics of interacting diseases. *Phys. Rev. X* **4**, 041005 (2014).
51. Ahn, Y.-Y., Jeong, H., Masuda, N. & Noh, J. D. Epidemic dynamics of two species of interacting particles on scale-free networks. *Phys. Rev. E* **74**, 066113 (2006).

52. Rodriguez, J. P., Liang, Y.-H., Huang, Y.-J. & Juang, J. Diversity of hysteresis in a fully cooperative coinfection model. *Chaos* **28**, 023107 (2018).
53. Pastor-Satorras, R., Castellano, C., Van Mieghem, P. & Vespignani, A. Epidemic processes in complex networks. *Rev. Mod. Phys.* **87**, 925–979 (2015).
54. Zhou, D. et al. Simultaneous first- and second-order percolation transitions in interdependent networks. *Phys. Rev. E* **90**, 012803 (2014).
55. Baxter, G., Dorogovtsev, S., Lee, K.-E., Mendes, J. & Goltsev, A. Critical dynamics of the k-core pruning process. *Phys. Rev. X* **5**, 031017 (2015).
56. Lee, D., Choi, S., Stippinger, M., Kertész, J. & Kahng, B. Hybrid phase transition into an absorbing state: Percolation and avalanches. *Phys. Rev. E* **93**, 042109 (2016).
57. Strogatz, S. H. *Nonlinear Dynamics and Chaos: With Applications to Physics, Biology, Chemistry, and Engineering* (Westview Press, Boulder, 2014).
58. Sadilek, M. & Thurner, S. Physiologically motivated multiplex Kuramoto model describes phase diagram of cortical activity. *Sci. Rep.* **5**, 10015 (2015).
59. Castellano, C., Fortunato, S. & Loreto, V. Statistical physics of social dynamics. *Rev. Mod. Phys.* **81**, 591 (2009).

### Acknowledgements

M.D. thanks the Azrieli Foundation for the award of an Azrieli Fellowship Grant. S.H. acknowledges the Israel Science Foundation, ONR Global, the Israel-Italian collaborative project NECST, Japan Science Foundation, BSF-NSF, and DTRA (Grant no. HDTRA-1-10-1-0014) for financial support. S.H. also thanks the Nvidia Corporation for a small

hardware grant, which was used for this research. This work was supported by the Israeli Ministry of Science, Technology and Space (MOST grant #3-12072). We also thank B. Barzel, A.K.H. Chan and V. Zlatic for several helpful comments and discussions about the manuscript.

### Author contributions

M.M.D., I.B., S.B. and S.H. developed the concept. I.B. and M.M.D. jointly designed the framework. I.B. developed the analytic results. M.M.D. created all of the simulations and figures. S.B. provided conceptual advice. M.M.D., I.B. and S.H. wrote the paper.

### Competing interests

The authors declare no competing interests.

### Additional information

**Supplementary information** is available for this paper at <https://doi.org/10.1038/s41567-018-0343-1>.

**Reprints and permissions information** is available at [www.nature.com/reprints](http://www.nature.com/reprints).

**Correspondence and requests for materials** should be addressed to M.M.D.

**Publisher's note:** Springer Nature remains neutral with regard to jurisdictional claims in published maps and institutional affiliations.

© The Author(s), under exclusive licence to Springer Nature Limited 2018

## Methods

**Heterogeneous mean-field theory.** We sketch the main steps performed in deriving the system of equation (6), here generalized to the case of finite fractions of dependency links. For simplicity, let us consider a system of  $M=2$  interacting networks having factorized pairwise dynamics  $h(x_i, x_j) = h_1(x_i)h_2(x_j)$  (refs<sup>59,60</sup>), in which case equation (5) reads

$$\dot{x}_i^\sigma = g_i^\sigma(x_i^\sigma) + \lambda_\sigma \mathcal{D}_i^{\mu \rightarrow \sigma} h_1^\sigma(x_i^\sigma) \sum_{j=1}^N A_{ij}^\sigma h_2^\sigma(x_j^\sigma) \quad (9)$$

The latter suggests the natural choice  $\mathcal{O}_\sigma \equiv h_2^\sigma$  for the ordering functions defined in equation (2). Searching for steady states, one can in principle solve equation (9) with self-consistent arguments by defining the auxiliary functions  $\mathcal{R}_i \equiv -g_i/h_1$  for each node in each layer. Steady solutions hence have the form  $\mathcal{R}_i^\sigma(x_i^\sigma) = \lambda_\sigma k_i^\sigma \mathcal{D}_i^{\mu \rightarrow \sigma} z_i^\sigma$ , which (assuming that each  $\mathcal{R}_i$  is invertible) lead to self-consistent equations for each  $z_i^\sigma$ :

$$z_i^\sigma = \frac{1}{k_i^\sigma} \sum_{j=1}^N A_{ij}^\sigma \mathcal{Q}_i^\sigma (\lambda_\sigma k_i^\sigma \mathcal{D}_i^{\mu \rightarrow \sigma} z_i^\sigma) \quad (10)$$

where  $\mathcal{Q}_i \equiv h_2 \mathcal{R}_i^{-1}$  (see Supplementary equation (11) and details therein). To reduce the computational complexity of the problem and allow analytical tractability, we consider an ensemble of uncorrelated random graphs with prescribed degree sequences<sup>61–64</sup>. Adopting the so-called annealed network approximation<sup>65–67</sup>, we thus replace the entries of the adjacency matrices with their graph-ensemble averages, so that

$$A_{ij}^\sigma \xrightarrow{\text{ann.netw.approx.}} \langle A_{ij}^\sigma \rangle_\sigma \equiv p_{ij}^\sigma \simeq \frac{k_i^\sigma k_j^\sigma}{N \langle k \rangle_\sigma} \quad (11)$$

where  $p_{ij}^\sigma$  are the probabilities that vertices  $i$  and  $j$  with degree  $k_i^\sigma$  and  $k_j^\sigma$ , respectively, are connected in layer  $\sigma = A, B$ . In this approximation, each local order parameter (equation (2)) becomes independent of the node indices—that is  $z_i \equiv Z$  for every  $i = 1, \dots, N$ . Rearranging the sums in equation (10) and performing the thermodynamic limit ( $N \rightarrow \infty$ ), one eventually finds (see Supplementary equations (14)–(16)) the integral self-consistent equations

$$Z_\sigma = \int_{k_{\min}}^{+\infty} \frac{k P_\sigma(k)}{\langle k \rangle_\sigma} \int_{-\infty}^{+\infty} \Gamma^{\mu \rightarrow \sigma}(x, k) \mathcal{G}_\sigma(\lambda_\sigma Z_\sigma x, k) dx dk \quad (12)$$

where the function  $\mathcal{G}_\sigma$  depends on  $\mathcal{Q}_\sigma$  according to the mean-field solution of the single layer case, while  $\Gamma^{\mu \rightarrow \sigma}$  is the (generally degree-dependent) distribution of the dynamical dependencies  $\mathcal{D}^{\mu \rightarrow \sigma}$  between the networks. In the present work we discussed the special case of randomly distributed dependencies with constant probabilities  $f_A, f_B \in [0, 1]$ , whose distributions among nodes can be thus succinctly written as

$$\Gamma^{\mu \rightarrow \sigma}(x) = f_\sigma \delta(x - \mathcal{D}^{\mu \rightarrow \sigma}) + (1 - f_\sigma) \delta(x - 1) \quad (13)$$

where  $\delta(\cdot)$  is the Dirac delta distribution. We stress that, if  $f_A = f_B \equiv 1$  (that is fully dependent networks), we actually recover the self-consistent equation (6).

**Reduced dynamics for two interacting networks of phase oscillators.** Consider the system of equations

$$\dot{\theta}_i^\sigma = \omega_i^\sigma + \lambda_\sigma \mathcal{D}_i^{\mu \rightarrow \sigma} k_i^\sigma (\mathcal{B}_i^\sigma + \text{Im}\{\mathcal{W}_i^\sigma e^{-i\theta_i^\sigma}\}) \quad (14)$$

where  $\mathcal{B}_i^\sigma, \mathcal{W}_i^\sigma$  depend on local properties of oscillators (for example, local order  $z_i \equiv r_i e^{i\psi_i}$ , connectivity, shear and so on), but not on the phases themselves. The system of equations (14) describes a broad family of coupled phase oscillator models, including neuronal models, Stuart–Landau oscillators, the Winfree model, and indeed the Kuramoto dynamics given by equation (7).

Adopting the Ott–Antonsen reduction<sup>68</sup>, we derive in Supplementary Section 2 the equations for the low-dimensional dynamics of the model (equation (14)), which asymptotically attract the collective evolution of the system in the annealed approximation (equation (11)). For explanatory purposes, we considered there the case of interacting Winfree oscillators (see Supplementary equations (20)–(24))<sup>69</sup>, whose low-dimensional dynamics reduce to

$$\begin{aligned} A_\sigma + i\omega_\sigma A_\sigma + \frac{1}{2} \lambda_\sigma k x (Z_\sigma A_\sigma - \overline{Z_\sigma}) &= 0 \\ Z_\sigma &= \int_{k_{\min}}^{+\infty} \frac{k P_\sigma(k)}{\langle k \rangle_\sigma} \int_{-\infty}^{+\infty} \Gamma^{\mu \rightarrow \sigma}(x, k) \mathcal{G}_\sigma(k, x, t) dk dx \\ \mathcal{G}_\sigma(k, x, t) &\equiv \int_{-\infty}^{+\infty} u_\sigma(\omega) \overline{A_\sigma}(\omega, k, x, t) d\omega \end{aligned} \quad (15)$$

in the limit of weak couplings (see Supplementary Information for details). The system in equation (15) models the asymptotic evolution of the global order parameters  $Z_\sigma = R_\sigma e^{i\psi_\sigma}$  for the Kuramoto model (equation (7)).

Stationary solutions of the system in equation (15) yield all the collective states of the model in equation (7) with time-independent coherences and frequencies  $\Omega_\sigma \equiv \psi_\sigma$ . Because states with  $R_\sigma > 0$  can be stationary only in reference frames co-rotating with their mean-fields<sup>70</sup>, we perform the transforms  $u_\sigma(\omega) \mapsto u_\sigma(\omega + \Omega_\sigma)$  which leave invariant equation (7). Imposing the stationarity conditions  $\partial_t Z_\sigma = 0$  in the system of equation (15), we find

$$A_\sigma = e^{-i\psi_\sigma} \begin{cases} \frac{-i\omega}{\lambda_\sigma k R_\sigma x} + \sqrt{1 - \left( \frac{\omega}{\lambda_\sigma k R_\sigma x} \right)^2} & |\omega| \leq \lambda_\sigma k R_\sigma x \\ \frac{-i\omega}{\lambda_\sigma k R_\sigma x} \left[ 1 - \sqrt{1 - \left( \frac{\lambda_\sigma k R_\sigma x}{\omega} \right)^2} \right] & \text{otherwise} \end{cases}$$

describing, respectively, phase-locked and drifting oscillators' contributions (see Supplementary Equation (29)) to the order parameters of each subsystem<sup>71</sup>. Substituting the latter solutions into equation (15) and equating real and imaginary parts of the expressions obtained, we find a system of four self-consistent equations for  $(R_\sigma, \Omega_\sigma, R_B, \Omega_B)$  (Supplementary Equations (30–33)). In particular, assuming symmetric and unimodal natural frequency distributions  $u_\sigma$ , two of the previous four equations simplify to  $\Omega_\sigma = \langle \omega \rangle_\sigma$ , where  $\langle \omega \rangle_\sigma \equiv \int \omega u_\sigma(\omega) d\omega$ .

Notice that, even for symmetric and unimodal  $u_\sigma$ , there will always be travelling wave states (that is, stationary solutions of equation (15) with  $\Omega_\sigma \neq 0$ ) in one of the two layers. Being an artefact of the choice of the rotating reference frame and having hence no physical relevance, we can further assume that both  $u_\sigma$  have vanishing mean, so that  $\Omega_\sigma = 0$  for  $\sigma = A, B$ . These assumptions drastically simplify the analysis of the model (equation (7)), reducing the system of self-consistent equations (15) to

$$R_\sigma = \int_{k_{\min}}^{+\infty} \frac{k P_\sigma(k)}{\langle k \rangle_\sigma} \int_{-\infty}^{+\infty} \Gamma^{\mu \rightarrow \sigma}(x, k) \mathcal{G}_\sigma^{\text{Kura}}(\lambda_\sigma R_\sigma x, k) dx dk$$

where  $\mathcal{G}_\sigma^{\text{Kura}}$  has the form introduced above, following equation (7).

The null solution  $R_A = R_B = 0$ , describing mutual incoherence, is always a trivial fixed point of the above system of equations, which can be stable or unstable depending on the choice of parameters in the phase diagram. Non-vanishing solutions can be instead found numerically for particular network topologies and frequency distributions, once the strategy for the dynamical interactions between the layers has been chosen. In Supplementary Section 2.2, we have analysed the cases of equal ER networks, first with uniform and then with Cauchy–Lorentz frequency distributions.

## Data availability

The data that support the plots within this paper and other findings of this study are available from the corresponding author upon reasonable request.

## References

- Barzel, B., Liu, Y.-Y. & Barabási, A.-L. Constructing minimal models for complex system dynamics. *Nat. Commun.* **6**, 7186 (2015).
- Bollobás, B. *Random Graphs* 2nd edn, 7186 (Cambridge Univ. Press, Cambridge, 2001).
- Newman, M. *Networks: An Introduction* (Oxford Univ. Press, Oxford, 2010).
- Cohen, R. & Havlin, S. *Complex Networks: Structure, Robustness and Function* (Cambridge Univ. Press, Cambridge, 2010).
- Bianconi, G. Statistical mechanics of multiplex networks: Entropy and overlap. *Phys. Rev. E* **87**, 062806 (2013).
- Dorogovtsev, S. N., Goltsev, A. V. & Mendes, J. F. F. Critical phenomena in complex networks. *Rev. Mod. Phys.* **80**, 1275–1335 (2008).
- Boccalletti, S. et al. The structure and dynamics of multilayer networks. *Phys. Rep.* **544**, 1–122 (2014).
- Porter, M. A. & Gleeson, J. P. *Dynamical Systems on Networks: A Tutorial* Vol. 544, 1–122 (Springer, Cham, 2016).
- Pietras, B. & Daffertshofer, A. Ott–Antonsen attractiveness for parameter-dependent oscillatory systems. *Chaos* **26**, 103101 (2016).
- Pazó, D. & Montbrío, E. Low-dimensional dynamics of populations of pulse-coupled oscillators. *Phys. Rev. X* **4**, 011009 (2014).
- Iatsenko, D., Petkoski, S., McClintock, P. & Stefanovska, A. Stationary and traveling wave states of the Kuramoto model with an arbitrary distribution of frequencies and coupling strengths. *Phys. Rev. Lett.* **110**, 064101 (2013).
- Rodrigues, F. A., Peron, T. K. D., Ji, P. & Kurths, J. The Kuramoto model in complex networks. *Phys. Rep.* **610**, 1–98 (2016).